

# Torsional oscillations of neutron stars in scalar-tensor theory of gravity

Hector O. Silva,<sup>1,\*</sup> Hajime Sotani,<sup>2,†</sup> Emanuele Berti,<sup>1,‡</sup> and Michael Horbatsch<sup>1,3,§</sup>

<sup>1</sup>*Department of Physics and Astronomy, The University of Mississippi, University, MS 38677, USA*

<sup>2</sup>*Division of Theoretical Astronomy, National Astronomical*

*Observatory of Japan, 2-21-1 Osawa, Mitaka, Tokyo 181-8588, Japan*

<sup>3</sup>*School of Physics and Astronomy, University of Nottingham, Nottingham, NG7 2RD, UK*

(Dated: September 8, 2018)

We study torsional oscillations of neutron stars in the scalar-tensor theory of gravity using the relativistic Cowling approximation. We compute unperturbed neutron star models adopting realistic equations of state for the neutron star’s core and crust. For scalar-tensor theories that allow for spontaneous scalarization, the crust thickness can be significantly smaller than in general relativity. We derive the perturbation equation describing torsional oscillations in scalar-tensor theory, and we solve the corresponding eigenvalue problem to find the oscillation frequencies. The fundamental mode (overtone) frequencies become smaller (larger) than in general relativity for scalarized stellar models. Torsional oscillation frequencies may yield information on the crust microphysics *if* microphysics effects are not degenerate with strong-gravity effects, such as those due to scalarization. To address this issue, we consider two different models for the equation of state of the crust and we look at the effects of electron screening. The effect of scalarization on torsional oscillation frequencies turns out to be smaller than uncertainties in the microphysics for all spontaneous scalarization models allowed by binary pulsar observations. Our study shows that the observation of quasi-periodic oscillations (QPOs) following giant flares can be used to constrain the microphysics of neutron star crusts, whether spontaneous scalarization occurs or not.

PACS numbers: 04.40.Dg, 97.60.Jd, 04.50.Kd, 04.80.Cc

## I. INTRODUCTION

Observations of quasi-periodic oscillations (QPOs) following giant flares in soft gamma-ray repeaters [1–3] suggest a close coupling between the seismic motion of the crust after a major quake and the modes of oscillations in a magnetar. The analysis of X-ray data in SGR 1900+14 [2] and SGR 1806-20 [3] has unveiled a number of periodicities, with frequencies that agree reasonably well with the expected torsional (or toroidal shear) oscillation modes of the neutron star (NS) crust: see e.g. [4] for a review, and [5] for recent progress in explaining apparent discrepancies between theoretical models and observations. These observations are very exciting because they allow us, for the very first time, to test NS oscillation models.

The foundations of crustal torsional oscillation theory in general relativity (GR) were laid in a classic paper by Schumaker and Thorne [6]. Recent work motivated by QPO observations explored how torsional oscillation frequencies are affected by various physical effects, including crustal elasticity [7], magnetic fields [8–10], superfluidity [11], the nuclear symmetry energy [12–14] and electron screening [15].

The main motivation of this paper is to answer the following question: could torsional oscillation frequencies carry observable imprints of strong-field dynamics,

and possibly hint at dynamics beyond GR? Vice versa, can we ignore effects due to hypothetical strong-field modifications of GR when we explore the dependence of torsional oscillation frequencies on the various physical mechanisms listed above?

We address these questions within the simplest class of modifications of GR, namely scalar-tensor theory. Damour and Esposito-Farèse [16] showed that a wide class of scalar-tensor theories can pass Solar System tests and exhibit nonperturbative strong-field deviations away from GR (“spontaneous scalarization”) that can potentially be measured by observations of the bulk properties of NSs, and of binary systems containing NSs. The magnitude of these deviations is very sensitive to the value of a certain theory parameter  $\beta$ , defined in Eq. (16) below<sup>1</sup>.

Static NSs in theories with spontaneous scalarization were first studied in [16]. Their stability was investigated using catastrophe theory by Harada [17, 18]. The formation of scalarized NSs in gravitational collapse was studied in [19, 20], and a possible mechanism to “seed” macroscopic scalar fields from quantum vacuum instabilities was recently suggested [21–23]. Slowly rotating NSs were studied at first [24, 25] and second [26] order in rotation by extending the Hartle-Thorne formalism [27, 28]. Recent work [29–31] addressed the properties of rapidly rotating NS models.

Widely-separated binary systems of compact objects in scalar-tensor theory have been studied in [24, 32, 33],

\* hosilva@phy.olemiss.edu

† sotani@yukawa.kyoto-u.ac.jp

‡ eberti@olemiss.edu

§ mhorbats@olemiss.edu

<sup>1</sup> There exists a threshold  $\beta_c \sim -4.5$ , whose exact value depends on the NS equation of state. Scalarization is possible when  $\beta < \beta_c$ .

and the results have been combined with binary pulsar timing data in order to obtain bounds on scalar-matter coupling parameters, in particular  $\beta$ . Recent pulsar timing data continue to improve these bounds [34, 35]. Recently there has been interest in close binaries and mergers, and it was found that *dynamical scalarization* may take place: a close NS binary may scalarize even if the NSs would not scalarize in isolation [36–38]. The possibility of exploiting this mechanism in order to obtain bounds on scalar-matter coupling parameters from future gravitational wave observations has been explored in [39, 40].

A second motivation for this work comes from the surprising finding that there are universal “I-Love-Q” relations between a NS’s moment of inertia, tidal Love number and quadrupole moment in GR [41, 42]. These relations are “universal” in the sense that they are independent of the poorly known equation of state (EOS) of matter at high densities. Yagi and Yunes [41, 42] pointed out that if these relations were different in alternative theories of gravity, measurements of these bulk NS properties could be used to constrain alternative theories or even hint at possible strong-field modifications of GR. However, stellar structure calculations in scalar-tensor theories show that the I-Love-Q relations are remarkably insensitive to scalarization for values of the theory parameters allowed by binary pulsar tests [26, 31]. If the static properties of NSs (multipole moments and tidal deformation coefficients) cannot be used for this purpose, it seems natural to explore QPOs and torsional oscillation frequencies as promising observational avenues to look for smoking guns of new physics.

Several papers have investigated the signature of alternative theories of gravity on the NS oscillation spectrum. Sotani et al. studied nonradial oscillations in scalar-tensor gravity [43–45], TeVeS [46–49] and Eddington-inspired Born-Infeld gravity [50]. In particular, Refs. [43, 44] showed that the nonradial oscillation frequencies of NSs can change when the effects of scalarization are large enough to modify the bulk properties of the star by an appreciable amount. These studies were motivated by gravitational-wave asteroseismology, i.e. by the prospect of constraining the stellar properties and the EOS from direct observations of gravitational radiation from oscillating NSs. This is one of the major science goals of third-generation gravitational-wave detectors such as the Einstein Telescope, but it seems highly unlikely that we will measure NS oscillation accurately enough to constrain alternative theories of gravity with upcoming second-generation experiments, such as Advanced LIGO and Virgo (cf. [51, 52] for reviews). The connection between torsional oscillations and QPOs means that our results have more immediate experimental relevance.

Another noteworthy aspect of this work is that, whereas models of NSs in alternative theories of gravity usually adopt simple EOS models, none of these investigations have studied the effect of scalarization on the structure of the NS crust. Here we show quantitatively

the connection between the crustal depth, the threshold for scalarization and the scalar field profile in a scalarized star.

The plan of the paper is as follows. In Sec. II we give the equations of hydrostatic equilibrium and we present numerical results for the equilibrium structure using different models for the EOS prevailing in the crust. In Sec. III we derive the perturbation equation describing torsional oscillations in scalar-tensor theory in the Cowling approximation, and we describe the numerical method we used to solve the corresponding eigenvalue problem. Sec. IV shows our numerical results for the oscillation spectra. In the conclusions we discuss the implications and possible extensions of our work. Appendix A provides the derivation of an approximate analytical expression for the ratio between the crust thickness and the stellar radius in scalar-tensor theory, that generalizes a similar result by Samuelsson and Andersson [7] in GR. We carry out most of the work in the Einstein frame, but in Appendix B we show that the Einstein- or Jordan-frame formulations are equivalent, in the sense that the energy-momentum conservation law in either frame leads to the same perturbation equations.

## II. STELLAR MODELS IN SCALAR-TENSOR THEORY

### A. Action and field equations

We consider the Einstein-frame action [16]

$$S = \frac{c^4}{16\pi G_*} \int d^4x \frac{\sqrt{-g_*}}{c} (R_* - 2g_*^{\mu\nu} \partial_\mu \varphi \partial_\nu \varphi) + S_M[\psi_M; A^2(\varphi)g_{*\mu\nu}], \quad (1)$$

where  $G_*$  is the bare gravitational constant,  $g_* \equiv \det[g_{*\mu\nu}]$  is the determinant of the Einstein-frame metric  $g_{*\mu\nu}$ ,  $R_*$  is the Ricci curvature scalar of the metric  $g_{*\mu\nu}$  and  $\varphi$  is a massless scalar field.  $S_M$  is the action of the matter fields  $\psi_M$ , coupled to the Einstein-frame metric  $g_{*\mu\nu}$  and scalar field  $\varphi$  via the Jordan-frame metric  $\tilde{g}_{\mu\nu} \equiv A^2(\varphi)g_{*\mu\nu}$ , where  $A(\varphi)$  is a conformal factor. Throughout this work we use geometrical units ( $c = 1 = G_*$ ) and a mostly plus metric signature  $(-, +, +, +)$ . Quantities associated with the Einstein (Jordan) frame will be labeled with an asterisk (tilde).

The field equations of this theory, obtained by varying the action  $S$  with respect to  $g_*^{\mu\nu}$  and  $\varphi$ , respectively, are given by

$$R_{*\mu\nu} = 2\partial_\mu \varphi \partial_\nu \varphi + 8\pi \left( T_{*\mu\nu} - \frac{1}{2} T_* g_{*\mu\nu} \right), \quad (2)$$

$$\square_* \varphi = -4\pi \alpha(\varphi) T_*, \quad (3)$$

where  $R_{*\mu\nu}$  is the Ricci tensor,  $\alpha(\varphi) \equiv d \log A(\varphi) / d\varphi$  is usually called the “scalar-matter coupling function”,  $T_*^{\mu\nu}$

is the matter field energy-momentum tensor defined as

$$T_*^{\mu\nu} \equiv \frac{2}{\sqrt{-g_*}} \frac{\delta S_M[\psi_M, A^2(\varphi)g_{*\mu\nu}]}{\delta g_{*\mu\nu}}, \quad (4)$$

and  $T_* \equiv T_*^{\mu\nu} g_{*\mu\nu}$  is its trace. The energy-momentum tensor in the Jordan frame  $\tilde{T}^{\mu\nu}$ , with trace  $\tilde{T} \equiv \tilde{T}^{\mu\nu} \tilde{g}_{\mu\nu}$ , is defined as

$$\tilde{T}^{\mu\nu} \equiv \frac{2}{\sqrt{-\tilde{g}}} \frac{\delta S_M[\psi_M, \tilde{g}_{\mu\nu}]}{\delta \tilde{g}_{\mu\nu}}. \quad (5)$$

The energy-momentum tensors (and their traces) in these two conformally related representations of the theory are related as follows:

$$\begin{aligned} T_*^{\mu\nu} &= A^6(\varphi) \tilde{T}^{\mu\nu}, & T_{*\mu\nu} &= A^2(\varphi) \tilde{T}_{\mu\nu}, \\ T_* &= A^4(\varphi) \tilde{T}. \end{aligned} \quad (6)$$

Moreover, the covariant divergence of the energy-momentum tensor in the Einstein and Jordan frames can be shown to be

$$\nabla_{*\mu} T_*^{\mu\nu} = \alpha(\varphi) T_* \nabla_*^\nu \varphi, \quad (7)$$

$$\tilde{\nabla}_\mu \tilde{T}^{\mu\nu} = 0. \quad (8)$$

In the limit  $\alpha(\varphi) \rightarrow 0$  the scalar field decouples from matter, and the theory reduces to GR.

## B. The equations of hydrostatic equilibrium

The line element describing the space-time of a static, spherically symmetric star in Schwarzschild coordinates is given by

$$ds_*^2 = -e^{2\Phi} dt^2 + e^{2\Lambda} dr^2 + r^2 d\theta^2 + r^2 \sin^2 \theta d\phi^2 \quad (9)$$

in the Einstein frame, and by

$$\begin{aligned} d\tilde{s}^2 &= A^2(\varphi) (-e^{2\Phi} dt^2 + e^{2\Lambda} dr^2 + r^2 d\theta^2 \\ &\quad + r^2 \sin^2 \theta d\phi^2) \end{aligned} \quad (10)$$

in the Jordan frame, where  $\Phi$  and  $\Lambda$  are functions of the radial coordinate  $r$ . By symmetry, the scalar field  $\varphi$  also depends only on  $r$ . We assume the energy-momentum tensor  $\tilde{T}_{\mu\nu}$  to be that of a perfect fluid:

$$\tilde{T}_{\mu\nu} = (\tilde{\varepsilon} + \tilde{p}) \tilde{u}_\mu \tilde{u}_\nu + \tilde{p} \tilde{g}_{\mu\nu}, \quad (11)$$

where  $\tilde{\varepsilon}$  is the energy density,  $\tilde{p}$  the pressure and  $\tilde{u}_\mu$  the fluid's four-velocity. Using Eqs. (9) and (11), the field equations (2) and (3) yield the following equations that describe a static spherically symmetric star in hydrostatic

equilibrium in scalar-tensor theory [16, 24]:

$$\frac{dm}{dr} = 4\pi A^4(\varphi) r^2 \tilde{\varepsilon} + \frac{1}{2} r(r-2m) \psi^2, \quad (12)$$

$$\frac{d\Phi}{dr} = 4\pi A^4(\varphi) \frac{r^2 \tilde{p}}{r-2m} + \frac{1}{2} r \psi^2 + \frac{m}{r(r-2m)}, \quad (13)$$

$$\begin{aligned} \frac{d\psi}{dr} &= 4\pi A^4(\varphi) \frac{r}{r-2m} [\alpha(\varphi)(\tilde{\varepsilon} - 3\tilde{p}) + r(\tilde{\varepsilon} - \tilde{p})\psi] \\ &\quad - \frac{2(r-m)}{r(r-2m)} \psi, \end{aligned} \quad (14)$$

$$\frac{d\tilde{p}}{dr} = -(\tilde{\varepsilon} + \tilde{p}) \left[ \frac{d\Phi}{dr} + \alpha(\varphi)\psi \right]. \quad (15)$$

Here  $m = m(r)$  is the relativistic mass-energy function, defined in terms of  $\Lambda(r)$  as  $m \equiv (r/2)(1 - e^{-2\Lambda})$ , and we introduced  $\psi \equiv d\varphi/dr$ .

Hereafter, following Damour and Esposito-Farèse [16, 24], we will focus on the scalar-tensor theory specified by the choice

$$A(\varphi) = e^{\frac{1}{2}\beta\varphi^2}. \quad (16)$$

For sufficiently large and negative values of  $\beta$ , as discussed in the introduction, NSs in this theory can undergo a phase transition called *spontaneous scalarization* and acquire a nonvanishing scalar charge associated with a nontrivial scalar field configuration. These scalarized solutions of the field equations are more energetically favorable than non-scalarized solutions.

To close this system of equations we must complement it with an EOS  $\tilde{p} = \tilde{p}(\tilde{\varepsilon})$ . In this paper, we construct our stellar models adopting two EOSs for the NS core, namely EOS APR [53] and EOS MS0 [54], while for the NS crust we use the EOSs derived by Kobyakov and Pethick (henceforth KP, [55]) and by Douchin and Haensel (henceforth DH, [56]). These crust EOSs have densities  $\tilde{\varepsilon}_b$  at the crust basis equal to  $\tilde{\varepsilon}_b = 1.504 \times 10^{14}$  g/cm<sup>3</sup> for EOS KP, and  $\tilde{\varepsilon}_b = 1.285 \times 10^{14}$  g/cm<sup>3</sup> for EOS DH. For a comparison between the physical assumptions involved in the construction of these two EOSs, see e.g. [15]. In Fig. 1 we display the relation between pressure and energy density for EOSs DH and KP.

## C. Numerical results for unperturbed stars

To obtain the equilibrium stellar models we integrate numerically Eqs. (12)-(15) outwards starting from  $r = 0$  with initial conditions  $m(0) = 0$ ,  $\Phi(0) = \Phi_c$ ,  $\varphi(0) = \varphi_c$ ,  $\psi(0) = 0$  and  $\tilde{\varepsilon}(0) = \tilde{\varepsilon}_c$ , using one of the two EOSs (APR or MS0) for the core region. The point  $r = r_b$  such that  $\tilde{\varepsilon}(r_b) = \tilde{\varepsilon}_b$  determines the location of the crust basis. The integration then proceeds until we reach a point  $r = r_s$  for which  $\tilde{p}(r_s) = 0$ , which defines the Einstein-frame radius of the star. The radii  $r_b$  and  $r_s$  can be converted to the physical (Jordan) frame using the relations  $\tilde{R}_b = A(\varphi_b) r_b$  and  $\tilde{R} = A(\varphi_s) r_s$ , where  $\varphi_b = \varphi(r_b)$  and  $\varphi_s = \varphi(r_s)$ . We can then define the crust thickness

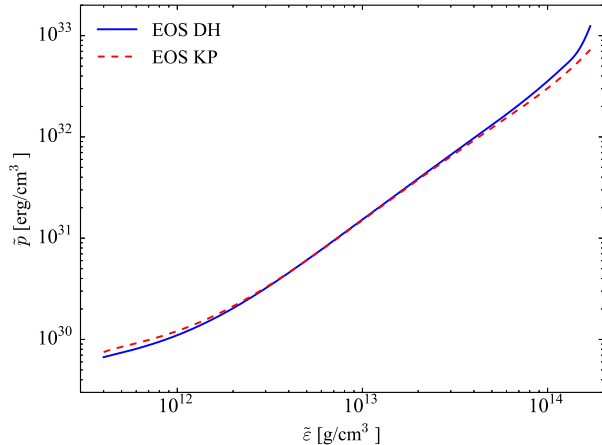


FIG. 1. (Color online) Pressure  $\tilde{p}$  versus energy density  $\tilde{\epsilon}$  for the crust EOSs considered in this work: EOS DH (solid line) and EOS KP (dashed line).

as  $\Delta\tilde{R} \equiv \tilde{R} - \tilde{R}_b$ . For convenience, we also introduce the dimensionless fractional crust thickness  $\tilde{\mathcal{R}} \equiv \Delta\tilde{R}/\tilde{R}$ . We remark that the theory is invariant under reflection symmetry ( $\varphi \rightarrow -\varphi$ ), and therefore, for simplicity, we shall only consider positive values of the scalar field.

At spatial infinity ( $r \rightarrow \infty$ ) the metric  $g_{*\mu\nu}$  and the scalar field  $\varphi$  behave asymptotically as

$$g_{*tt} = -1 + \frac{2M}{r} + \mathcal{O}\left(\frac{1}{r^2}\right), \quad (17)$$

$$g_{*rr} = 1 + \frac{2M}{r} + \mathcal{O}\left(\frac{1}{r^2}\right), \quad (18)$$

$$\varphi = \varphi_\infty + \frac{Q}{r} + \mathcal{O}\left(\frac{1}{r^2}\right), \quad (19)$$

where  $M$  is the ADM mass and  $Q$  is the scalar charge. The values of the various variables at the stellar surfaces (labeled with the subscript  $s$ ) can be used to calculate  $M$ ,  $Q$  and the asymptotic value of the scalar field  $\varphi_\infty \equiv \varphi(r \rightarrow \infty)$  via the following expressions [16]:

$$M = r_s^2 \Phi'_s \left(1 - \frac{2m_s}{r_s}\right)^{1/2} \exp\left\{-\frac{\Phi'_s}{(\Phi_s'^2 + \psi_s^2)^{1/2}}\right. \\ \left. \times \operatorname{arctanh}\left[\frac{(\Phi_s'^2 + \psi_s^2)^{1/2}}{\Phi'_s + 1/r_s}\right]\right\}, \quad (20)$$

$$Q = -\frac{\psi_s}{\Phi'_s} M, \quad (21)$$

$$\varphi_\infty = \varphi_s + \frac{\psi_s}{(\Phi_s'^2 + \psi_s^2)^{1/2}} \operatorname{arctanh}\left[\frac{(\Phi_s'^2 + \psi_s^2)^{1/2}}{\Phi'_s + 1/r_s}\right], \quad (22)$$

where  $\Phi'_s$  can be calculated with the aid of Eq. (13) as

$$\Phi'_s = \frac{1}{2} r_s \psi_s^2 + \frac{m_s}{r_s (r_s - 2m_s)}, \quad (23)$$

and primes indicate partial derivatives with respect to the radial coordinate  $r$ . From now on, we will assume that  $\varphi_\infty = 0$ .

To obtain solutions of Eqs. (12)-(15) satisfying this assumption, we apply the shooting method in order to find the central values of the scalar field  $\varphi_c$  such that the required value of  $\varphi_\infty$  is obtained. As a check of our code we compared our results against the ones presented in Refs. [30] (in scalar-tensor theory) and [57, 58] (in GR), finding excellent agreement.

In Fig. 2 we present general properties of stellar models constructed by solving Eqs. (12)-(15) combining EOS APR and EOS MS0 (for the NS core) with EOS KP and EOS DH (for the NS crust). The top row refers to the APR EOS, and the bottom row refers to the MS0 EOS; results for different crust models are shown using different line styles in each inset.

The leftmost column shows the mass-radius relation. Deviations from GR due to spontaneous scalarization are clearly visible; we also see that the choice of crustal EOS has negligible influence on the mass-radius relation, for both “ordinary” and scalarized stars. The second column shows the central value of the scalar field  $\varphi_c$  as a function of the central density  $\tilde{\epsilon}_c$ . The scalar field at the center acquires a nonzero value (i.e., the NS becomes scalarized) around  $\tilde{\epsilon}_c \approx 4 \times 10^{14} - 6 \times 10^{14} \text{ g/cm}^3$ , and it has a maximum around  $\tilde{\epsilon}_c \approx 7 \times 10^{14} - 9 \times 10^{14} \text{ g/cm}^3$ . In the third column we plot the dimensionless scalar charge  $\alpha \equiv -Q/M$  as a function of the compactness  $\tilde{\mathcal{C}} \equiv M/\tilde{R}$  (both expressed in geometrical units). Finally, the rightmost column shows  $\tilde{\mathcal{R}}$  as a function of the compactness  $\tilde{\mathcal{C}}$ . In comparison with their GR counterparts, for scalarized stars the crust represents a smaller fraction of the NS interior. Note also that deviations in the crust thickness due to scalarization and nonzero scalar charges develop in the same range of compactness  $\tilde{\mathcal{C}}$ , as expected.

These plots show that the choice of crustal EOS has negligible effects on the bulk properties of the star. This is not surprising, considering that EOSs DH and KP have very similar crust basis densities  $\tilde{\epsilon}_b$  and  $\tilde{p}(\tilde{\epsilon})$  (cf. Fig. 1). However, as we will see in Sec. III B, different crustal EOSs result in rather different elastic properties for the crust, and they do have an effect on torsional oscillation frequencies.

#### D. An approximate formula for $\mathcal{R}$

Samuelsson and Andersson [7] obtained a simple approximate analytical expression for the ratio between the crust thickness and stellar radius  $\mathcal{R}$ , within GR, in terms of the star’s compactness  $\mathcal{C}$ :

$$\mathcal{R} = \left(\frac{\mathcal{C}}{\sigma} e^{2\Lambda} + 1\right)^{-1}, \quad (24)$$

where  $e^{-2\Lambda} = 1 - 2\mathcal{C}$  and  $\sigma \approx 0.02326$  is a constant found by curve fitting, which in general depends on the crustal

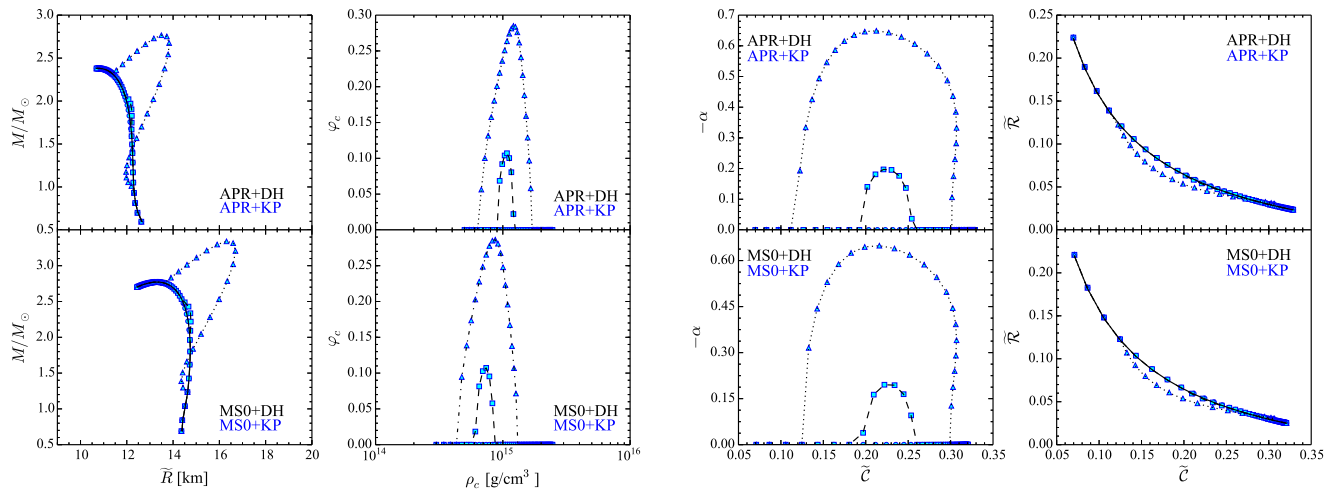


FIG. 2. (Color online) Properties of our stellar models in scalar-tensor theory. From left to right we show: the mass-radius relation, the scalar field at the center of the star  $\varphi_c$  as a function of the central density  $\bar{\varepsilon}_c$ , the dimensionless ratio  $-\alpha = Q/M$  as a function of the compactness  $\tilde{\mathcal{C}}$  and the fractional crust thickness  $\tilde{\mathcal{R}}$  as a function of  $\tilde{\mathcal{C}}$ . The choice of crustal EOS does not sensibly affect the crust thickness and the onset of scalarization. In all panels, curves with various linestyles correspond to stellar models using EOS DH for the NS crust: solid lines correspond to  $\beta = 0.0$ , dashed lines to  $\beta = -4.5$ , and dotted lines to  $\beta = -6.0$ . Different symbols correspond to stellar models using EOS KP for the crust: circles for  $\beta = 0.0$ , squares for  $\beta = -4.5$  and triangles for  $\beta = -6.0$ .

EOS [59].

In Appendix A we show that this result can be generalized to scalar-tensor theory as follows:

$$\mathcal{R} = \frac{\sigma}{2\beta\zeta} \left( \mathcal{F} - \sqrt{\mathcal{F}^2 - \frac{4\beta\zeta}{\sigma}} \right), \quad (25)$$

where we introduced

$$\mathcal{F} \equiv 1 + \frac{1}{\sigma} (\mathcal{C}e^{2\Lambda} + \beta\zeta) \quad (26)$$

and  $\zeta = \zeta(\mathcal{C}) \equiv \varphi_s \psi_s r_s$ , which is obtained by interpolation, given a family of stellar models, as a function of  $\mathcal{C}$ . We make the same approximations used in [7], and in addition we assume the scalar field to be constant throughout the NS crust. From Eq. (25) we can also calculate the first correction to Eq. (24) in powers of  $\beta\zeta$ , due the presence of the scalar field in a scalarized NS:

$$\mathcal{R} \approx \left( \frac{\mathcal{C}}{\sigma} e^{2\Lambda} + 1 \right)^{-1} - 2\mathcal{C}e^{2\Lambda} \frac{(\beta\zeta)^2}{\sigma^3} \left( \frac{\mathcal{C}}{\sigma} e^{2\Lambda} + 1 \right)^{-3}, \quad (27)$$

where the minus sign indicates that  $\mathcal{R}$  is smaller for such stars in comparison to nonscalarized ones, as observed in Figs. 2 and 3.

To illustrate how accurately Eq. (25) describes the behavior of  $\mathcal{R}$  observed in Fig. 2, in Fig. 3 we plot  $\mathcal{R}$ , choosing EOS APR to describe the NS core, as a function of  $\mathcal{C}$  for  $\beta = -6.0$  (the case in which deviations from GR are greatest). We find good agreement between the approximate expression and data obtained by numerically

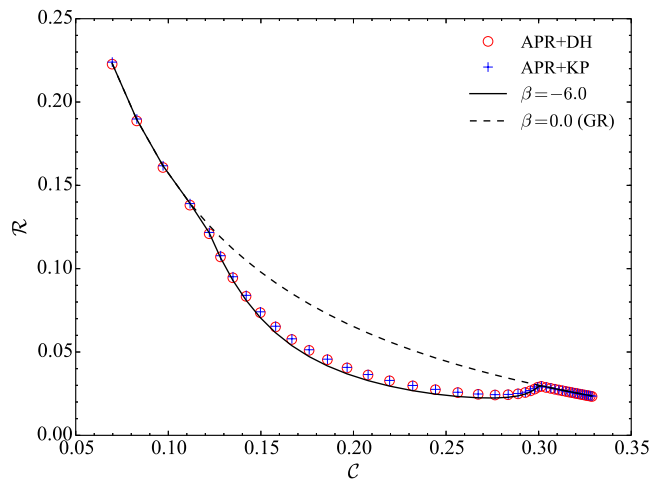


FIG. 3. (Color online) Comparison between Eq. (25) and the numerical results for  $\beta = -6.0$ , using  $\sigma = 0.02326$ . The GR expression (24) is also shown. Since the integration of Eqs. (12)-(15), gives us  $\varphi$  in the Einstein-frame radial coordinate  $r$ , the compactness and fractional crust thickness are evaluated in this frame. Notice, however, that even for  $\beta = -4.5$  (a value marginally excluded by binary pulsars observations [34]) the percent difference between the compactnesses and fractional crust thicknesses in the two frames is less than 1.0%, and therefore Eq. (25) is accurate for all physically sensible values of  $\beta$ .

solving Eqs. (12)-(15). As can be seen, the same value of  $\sigma$  obtained in [7] for the EOS used in [59] is accurate enough for both EOS DH and EOS KP.

### III. TORSIONAL PERTURBATIONS IN THE COWLING APPROXIMATION

#### A. Derivation of the perturbation equations

Let us now derive the equation describing torsional oscillations in scalar-tensor theory. We begin by introducing a small fluid perturbation described by a Lagrangian displacement vector

$$\tilde{\xi}^i = \left( 0, 0, \tilde{\mathcal{Y}}(t, r) \frac{1}{\sin \theta} \partial_\theta P_\ell(\cos \theta) \right), \quad (28)$$

where  $P_\ell(\cos \theta)$  is the Legendre polynomial of order  $\ell$ . For notational convenience, in Eq. (28) we omit the sum over  $\ell$ . The perturbation of the fluid four-velocity  $\delta \tilde{u}^3 = \tilde{u}^0(\partial \tilde{\xi}^3 / \partial t)$  is

$$\delta \tilde{u}^3 = A^{-1}(\varphi) e^{-\Phi} \dot{\tilde{\mathcal{Y}}}(t, r) \frac{1}{\sin \theta} \partial_\theta P_\ell(\cos \theta), \quad (29)$$

where the dot represents a partial derivative with respect to the time coordinate  $t$ .

In this work we use the Cowling approximation [60, 61], i.e. we assume that matter perturbations do not result in perturbations on the metric  $\tilde{g}_{\alpha\beta}$ :  $\delta \tilde{g}_{\mu\nu} = 0$ . Within this approximation, the perturbed perfect fluid energy-momentum tensor (11), including the shear tensor contribution  $\delta \tilde{S}_{\mu\nu}$ , is

$$\delta \tilde{T}_{\mu\nu} = (\tilde{p} + \tilde{\varepsilon}) (\delta \tilde{u}_\mu \tilde{u}_\nu + \tilde{u}_\mu \delta \tilde{u}_\nu) - 2\tilde{\mu} \delta \tilde{S}_{\mu\nu}, \quad (30)$$

as the pressure  $\tilde{p}$ , the energy density  $\tilde{\varepsilon}$  and the scalar field  $\varphi$  are unaffected by odd (axial) perturbations. We have also introduced the shear modulus  $\tilde{\mu} = \tilde{\mu}(r)$ . While the first term in Eq. (30) is simple to calculate, to obtain  $\delta \tilde{S}_{\mu\nu}$  we must first use the fact that  $\delta \tilde{\sigma}_{\mu\nu} \equiv \mathcal{L}_{\tilde{u}} \delta \tilde{S}_{\mu\nu} = A^{-1}(\varphi) \exp(-\Phi) \partial_0 \delta \tilde{S}_{\mu\nu}$ , where the perturbed rate of shear  $\delta \tilde{\sigma}_{\mu\nu} = \delta \tilde{\sigma}_{\nu\mu}$  is given by

$$\begin{aligned} \delta \tilde{\sigma}_{\mu\nu} = & \frac{1}{2} \left( \delta \tilde{P}_{\nu}^{\alpha} \tilde{\nabla}_{\alpha} \tilde{u}_{\mu} + \delta \tilde{P}_{\mu}^{\alpha} \tilde{\nabla}_{\alpha} \tilde{u}_{\nu} + \tilde{P}_{\nu}^{\alpha} \tilde{\nabla}_{\alpha} \delta \tilde{u}_{\mu} \right. \\ & \left. + \tilde{P}_{\mu}^{\alpha} \tilde{\nabla}_{\alpha} \delta \tilde{u}_{\nu} \right) - \frac{1}{3} \left( \delta \tilde{P}_{\mu\nu} \tilde{\nabla}_{\alpha} \tilde{u}^{\alpha} + \tilde{P}_{\mu\nu} \tilde{\nabla}_{\alpha} \delta \tilde{u}^{\alpha} \right), \end{aligned} \quad (31)$$

$\delta \tilde{P}_{\mu\nu}$  denotes the perturbed projection operator

$$\delta \tilde{P}_{\mu\nu} = \delta \tilde{u}_{\mu} \tilde{u}_{\nu} + \tilde{u}_{\mu} \delta \tilde{u}_{\nu}, \quad (32)$$

and  $\mathcal{L}_{\tilde{u}}$  is the Lie derivative along the worldline of a fluid element [6]. The nonzero components of the perturbed rate of shear  $\delta \tilde{\sigma}_{\mu\nu}$  can then be shown to be

$$\delta \tilde{\sigma}_{13} = \frac{1}{2} A(\varphi) e^{-\Phi} \dot{\tilde{\mathcal{Y}}}(t, r) r^2 \sin \theta \partial_\theta P_\ell(\cos \theta), \quad (33)$$

$$\delta \tilde{\sigma}_{23} = \frac{1}{2} A(\varphi) e^{-\Phi} \dot{\tilde{\mathcal{Y}}}(t, r) r^2 \sin^2 \theta \partial_\theta \left[ \frac{1}{\sin \theta} \partial_\theta P_\ell(\cos \theta) \right]. \quad (34)$$

Using Eqs. (33) and (34), the perturbed shear tensor has components

$$\delta \tilde{S}_{13} = \frac{1}{2} A^2(\varphi) \tilde{\mathcal{Y}}'(t, r) r^2 \sin \theta \partial_\theta P_\ell(\cos \theta), \quad (35)$$

$$\delta \tilde{S}_{23} = \frac{1}{2} A^2(\varphi) \tilde{\mathcal{Y}}'(t, r) r^2 \sin^2 \theta \partial_\theta \left[ \frac{1}{\sin \theta} \partial_\theta P_\ell(\cos \theta) \right]. \quad (36)$$

Combining these results, we find that the nonzero components of the perturbed energy-momentum tensor are

$$\delta \tilde{T}_{03} = -(\tilde{p} + \tilde{\varepsilon}) A^2(\varphi) \dot{\tilde{\mathcal{Y}}}(t, r) r^2 \sin \theta \partial_\theta P_\ell(\cos \theta), \quad (37)$$

$$\delta \tilde{T}_{13} = -\tilde{\mu} A^2(\varphi) \tilde{\mathcal{Y}}'(t, r) r^2 \sin \theta \partial_\theta P_\ell(\cos \theta), \quad (38)$$

$$\delta \tilde{T}_{23} = -\tilde{\mu} A^2(\varphi) \tilde{\mathcal{Y}}'(t, r) r^2 \sin^2 \theta \partial_\theta \left[ \frac{1}{\sin \theta} \partial_\theta P_\ell(\cos \theta) \right]. \quad (39)$$

In the GR limit – obtained by taking  $A(\varphi) = 1$ , and consequently  $\alpha(\varphi) = 0$  – the above results are in agreement with [6] when we neglect metric perturbations in their equations.

In the Cowling approximation, the variation of the energy-momentum conservation law in the Jordan frame [43] can be obtained from Eq. (8)

$$\begin{aligned} \tilde{\nabla}_{\nu} \delta \tilde{T}^{\nu}_{\mu} &= \partial_{\nu} \delta \tilde{T}^{\nu}_{\mu} + \Gamma_{*\alpha\nu}^{\nu} \delta \tilde{T}^{\alpha}_{\mu} - \Gamma_{*\mu\nu}^{\alpha} \delta \tilde{T}^{\nu}_{\alpha} \\ &+ 4\alpha(\varphi) \partial_{\alpha} \varphi \delta \tilde{T}^{\alpha}_{\mu} - \alpha(\varphi) \partial_{\mu} \varphi \delta \tilde{T}^{\alpha}_{\alpha} \\ &= 0, \end{aligned} \quad (40)$$

where  $\Gamma_{*\nu\sigma}^{\mu}$  denotes the Christoffel symbols of the Einstein-frame metric, related to they Jordan frame counterparts by

$$\tilde{\Gamma}_{\mu\nu}^{\sigma} = \Gamma_{*\mu\nu}^{\sigma} + \alpha(\varphi) (\delta_{\nu}^{\sigma} \partial_{\mu} \varphi + \delta_{\mu}^{\sigma} \partial_{\nu} \varphi - g_{*\rho}^{\sigma\rho} g_{*\mu\nu} \partial_{\rho} \varphi). \quad (41)$$

In Appendix B we show that Eq. (40) can also be obtained starting from the energy-momentum conservation law (7) in the Einstein frame, and therefore the two frames are physically equivalent.

By setting  $\mu = 3$  and making use of Eqs. (37)-(39) we obtain the following differential equation for  $\tilde{\mathcal{Y}}(t, r)$ :

$$\begin{aligned} \tilde{\mathcal{Y}}''(r) + \left[ \frac{4}{r} + \Phi' - \Lambda' + \frac{\tilde{\mu}'}{\tilde{\mu}} + 4\alpha(\varphi)\psi \right] \tilde{\mathcal{Y}}'(r) \\ + \left[ \left( \frac{\omega}{\tilde{v}_s} \right)^2 e^{-2\Phi} - \frac{(\ell+2)(\ell-1)}{r^2} \right] e^{2\Lambda} \tilde{\mathcal{Y}}(r) = 0, \end{aligned} \quad (42)$$

where we have assumed a harmonic time dependence  $\tilde{\mathcal{Y}}(t, r) = \tilde{\mathcal{Y}}(r) e^{i\omega t}$  for the perturbation variable, and we have introduced the shear wave velocity  $\tilde{v}_s^2 \equiv \tilde{\mu}/(\tilde{p} + \tilde{\varepsilon})$ .

We can recast Eq. (42) in a form identical to the GR case (cf. [6, 15]) if we introduce an effective shear modulus

$\tilde{\mu}_{\text{eff}} \equiv A^4(\varphi)\tilde{\mu}$ , an effective wave velocity  $\tilde{v}_{\text{eff}}^2 \equiv A^4(\varphi)\tilde{v}_s^2$  and a rescaled frequency  $\tilde{\omega} = A^2(\varphi)\omega$ :

$$\begin{aligned} \tilde{\mathcal{Y}}''(r) + \left[ \frac{4}{r} + \Phi' - \Lambda' + \frac{\tilde{\mu}'_{\text{eff}}}{\tilde{\mu}_{\text{eff}}} \right] \tilde{\mathcal{Y}}'(r) \\ + \left[ \left( \frac{\tilde{\omega}}{\tilde{v}_{\text{eff}}} \right)^2 e^{-2\Phi} - \frac{(\ell+2)(\ell-1)}{r^2} \right] e^{2\Lambda} \tilde{\mathcal{Y}}(r) = 0. \end{aligned} \quad (43)$$

Given the definition of the conformal factor (16), the factor  $A^4(\varphi)$  is always less than unity when  $\beta < 0$ , and therefore  $\tilde{\mu}_{\text{eff}}/\tilde{\mu} \leq 1$ .

To obtain the oscillation frequencies we must integrate Eq. (43) numerically with appropriate boundary conditions. We assume that torsional oscillations are confined to the NS crust, so our boundary conditions are a zero-torque condition at  $r = r_s$  and a zero-traction condition at  $r_b$ . These boundary conditions follow from the fact that the shear modulus is zero in the NS core and outside the star, and they imply that  $\tilde{\mathcal{Y}}(r)$  must satisfy Neumann boundary conditions, i.e.  $\tilde{\mathcal{Y}}'(r) = 0$  at both  $r = r_b$  and  $r = r_s$  [6, 8, 15]. Our integrations of Eq. (43) are performed in the Einstein frame, but since  $\varphi_\infty = 0$ , the torsional oscillation frequencies measured at infinity are the same in the Einstein and Jordan frames.

Following common practice in the literature, we will present numerical results for the torsional oscillation frequencies  $n t_\ell \equiv \omega/(2\pi)$ . Here  $n$  is the number of radial nodes of the function  $\tilde{\mathcal{Y}}(r)$  in the crust region, and  $\ell$  is the usual angular index associated with the Legendre polynomials  $P_\ell(\cos\theta)$ .

## B. The shear modulus

Torsional oscillations depend on the elastic properties of the solid NS crust [63], characterized by the shear stress tensor<sup>2</sup>. A crucial element in describing the elastic properties of the NS crust is the shear modulus  $\tilde{\mu}$ . Assuming the NS crust to be a body-centered cubic (bcc) lattice, Ogata and Ichimaru [64] (see also [65]) showed that the shear modulus in the limit of zero temperature can be approximated as

$$\tilde{\mu} = 0.1194 n \frac{(Ze)^2}{\tilde{a}}, \quad (44)$$

where  $n$  is the ion number density,  $Ze$  the charge of the nuclei and  $\tilde{a}^3 = 3/(4\pi n)$  is the radius of the Wigner-Seitz cell containing one nucleus. Although it is often assumed that the electrons are uniformly distributed in

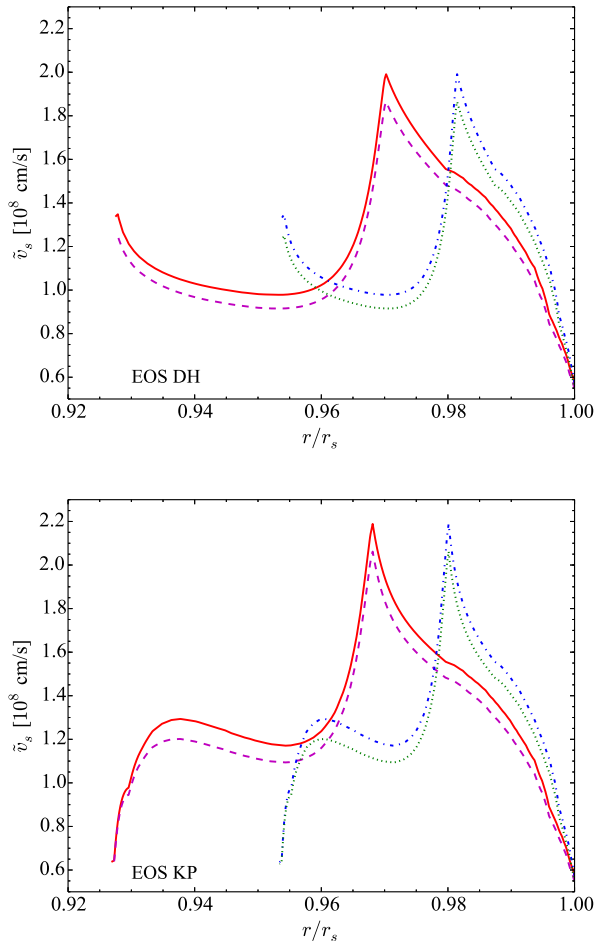


FIG. 4. (Color online) Shear velocity profile  $\tilde{v}_s(r)$  in the NS crust in the following cases: (i) GR without electron screening (solid line); (ii) GR with electron screening (dashed line); (iii) scalar-tensor theory ( $\beta = -6.0$ ) without electron screening (dashed-dotted line); (iv) scalar-tensor theory ( $\beta = -6.0$ ) with electron screening (dotted line). The top panel refers to EOS DH, the bottom panel to EOS KP. The sharp peaks occur near the neutron drip density  $\tilde{\varepsilon} \approx 3 \times 10^{11} \text{ g/cm}^3$  [62].

the NS crust, one can also calculate the correction to the shear modulus due a nonuniformity of the electron density distribution, i.e. electron screening effects [55, 66]. Kobayakov and Pethick [55] obtained the following electron screening correction term to Eq. (44):

$$\tilde{\mu} = 0.1194 n \left( 1 - 0.010 Z^{2/3} \right) \frac{(Ze)^2}{\tilde{a}}. \quad (45)$$

For  $Z = 40$ , electron screening can reduce the shear modulus by  $\approx 11.7\%$ . As discussed in [15], this reduces the fundamental mode frequency  ${}_0t_2$  by roughly 6% in GR, independently of whether we use EOS DH or KP.

In our calculations we consider both Eqs. (44) and (45) to see whether one would be able, in principle, to distinguish modifications of the torsional oscillations spectrum due a modified theory of gravity from microphysics effects

<sup>2</sup> Any deformation of an elastic medium can be decomposed into compressional and shear components. Matter in the NS crust is essentially incompressible, and this is why only a shear stress tensor is studied in the literature [63, 64].

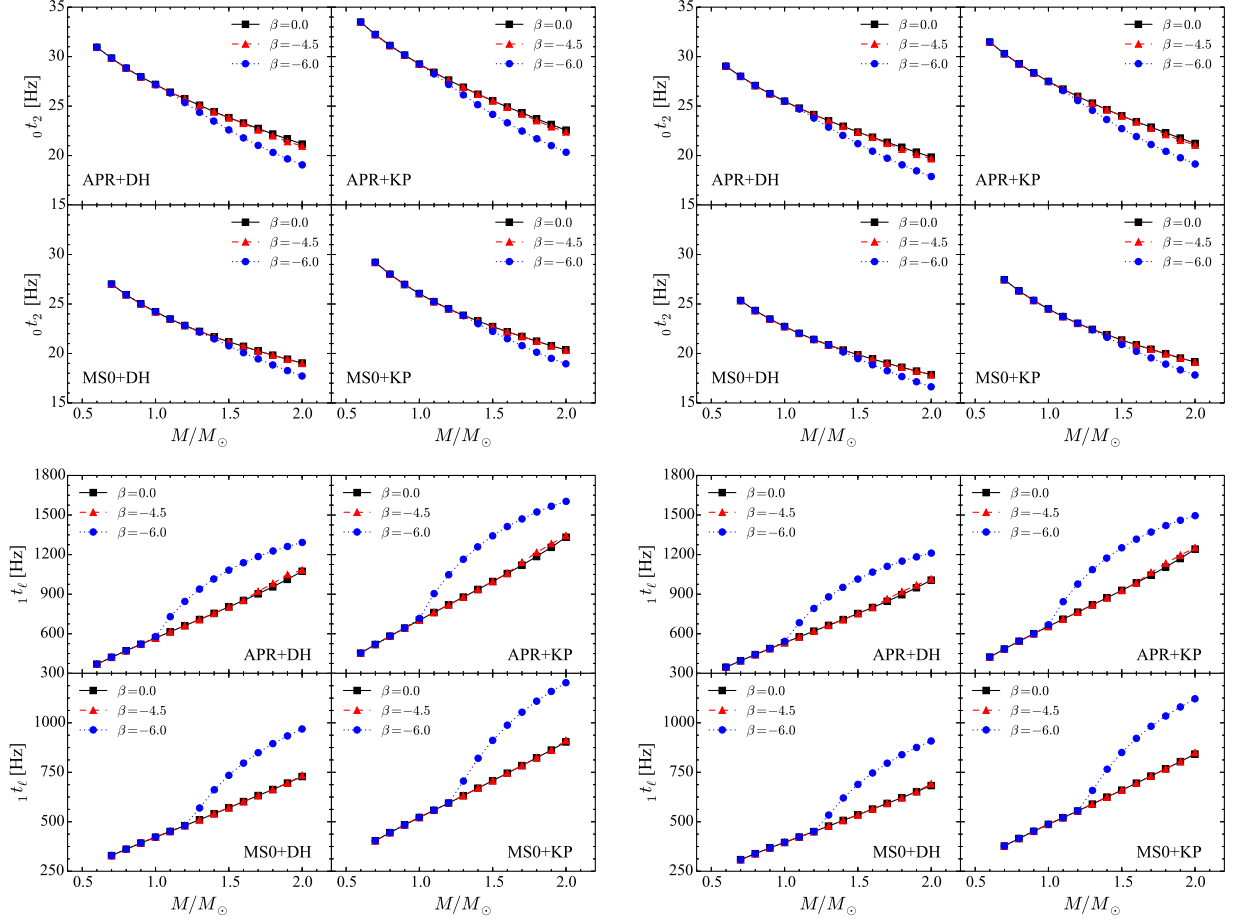


FIG. 5. (Color online) Frequencies of the torsional modes in scalar-tensor theory as a function of  $M/M_\odot$ . *Top panels:* the fundamental torsional mode  ${}_0t_2$  without (*left*) and with (*right*) electron screening. *Lower panels:* the first overtone  ${}_1t_1$  without (*left*) and with (*right*) electron screening.

(electron screening being one of the simplest examples to investigate).

The impact of electron screening effects can be visualized by plotting the shear velocity  $\tilde{v}_s^2 = \tilde{\mu}/(\tilde{\varepsilon} + \tilde{p})$  in the crust region. Fig. 4 shows  $\tilde{v}_s^2$  for NS models in GR and in a scalar-tensor theory with  $\beta = -6.0$ , using both EOS DH and KP, with and without electron screening effects. All NS models shown in the figure have radius  $R = 15.21$  km and mass  $M = 2.046 M_\odot$ . The (density-weighted) shear velocity

$$\langle \tilde{v}_s \rangle = \frac{\int_{r_b}^{r_s} \tilde{\varepsilon}(r) \tilde{v}_s(r) r^2 dr}{\int_{r_b}^{r_s} \tilde{v}_s(r) r^2 dr} \quad (46)$$

is always close to  $\approx 1 \times 10^8$  cm/s, in remarkable agreement with early estimates by Schumaker and Thorne [6] (see also [67]).

### C. Numerical procedure

To numerically integrate Eq. (42) and obtain the frequencies  ${}_n t_\ell$ , it is convenient to introduce two new variables  $\tilde{\mathcal{Y}}_1(r)$  and  $\tilde{\mathcal{Y}}_2(r)$ , defined as

$$\tilde{\mathcal{Y}}_1(r) \equiv r^{1-\ell} \tilde{\mathcal{Y}}(r), \quad (47)$$

$$\tilde{\mathcal{Y}}_2(r) \equiv \tilde{\mu}_{\text{eff}} e^{\Phi-\Lambda} r^{2-\ell} \tilde{\mathcal{Y}}'(r). \quad (48)$$

In terms of these variables, Eq. (42) can be decomposed into a system of two first-order coupled differential equations:

$$\begin{aligned} \tilde{\mathcal{Y}}_1'(r) &= -\frac{\ell-1}{r} \tilde{\mathcal{Y}}_1(r) + \frac{e^{\Lambda-\Phi}}{\tilde{\mu}_{\text{eff}} r} \tilde{\mathcal{Y}}_2(r), \\ \tilde{\mathcal{Y}}_2'(r) &= -\frac{\ell+2}{r} \tilde{\mathcal{Y}}_2(r) - e^{\Phi+\Lambda} [(\tilde{\varepsilon} + \tilde{p}) r \tilde{\omega}^2 e^{-2\Phi} \\ &\quad - (\ell+2)(\ell-1) \frac{\tilde{\mu}_{\text{eff}}}{r}] \tilde{\mathcal{Y}}_1(r). \end{aligned} \quad (49)$$

The advantage of this approach is that it eliminates the necessity of computing the derivative of the shear modulus  $\tilde{\mu}$ , which is known only in tabulated form. In terms of

$\tilde{\mathcal{Y}}_2(r)$ , the zero-traction and zero-torque conditions translate into the requirements that  $\tilde{\mathcal{Y}}_2(r_b) = \tilde{\mathcal{Y}}_2(r_s) = 0$ . The same change of variables was used in [8] in the context of magnetized stars (see also [68]).

Using Eqs. (49) and (50) we can now find the frequencies  ${}_n t_\ell$  by applying a shooting method (see e.g. [57]). Choosing  $\tilde{\mathcal{Y}}_1(r)$  to be normalized to unity, and setting  $\tilde{\mathcal{Y}}_2(r) = 0$  at the stellar surface  $r = R$ , we integrate Eqs. (12)-(15), (49) and (50) inwards for a trial value of  $\omega$  until we reach the crust basis at  $r = r_b$ , where we must have  $\tilde{\mathcal{Y}}_2(r_b) = 0$ . Depending on whether or not this condition is satisfied, we adjust the trial value of  $\omega$  until we find  $\tilde{\mathcal{Y}}_2(r_b) = 0$  within a certain tolerance. In this way the determination of  $\omega$  becomes a root finding problem, which can be solved using (for instance) the bisection method.

#### IV. THE OSCILLATION SPECTRA

With our equilibrium NS models and our numerical framework to deal with crustal perturbations, we are finally in a position to compute and discuss the spectrum of torsional oscillation frequencies in scalar-tensor theory. The spectrum depends quite sensitively on the bulk properties of the star (mass  $M$ , radius  $\tilde{R}$ , crust thickness  $\Delta\tilde{R}$ ), on the choice of crustal EOS, and on the scalar field profile in the crust region.

In Fig. 5 we show the torsional oscillation frequencies for the fundamental mode  ${}_0 t_2$  (top panels) and first overtone  ${}_1 t_2$  (bottom panels) as a function of the mass  $M$  for NS models with all possible combinations of core EOS (MS0, APR) and crust EOS (DH, KP). We show results for three different values of  $\beta$ :  $\beta = 0$  (GR),  $\beta = -4.5$  (marginally excluded by binary pulsar observations) and  $\beta = -6$  (observationally excluded, but shown nonetheless to maximize the effects of scalarization). By comparing the left and right panels we can quantify the influence of electron screening effects (everything else being the same): electron screening typically lowers the oscillation spectra, in agreement with the findings of Ref. [15]. For stellar models built using EOS MS0 and for the conservative value  $\beta = -4.5$ , modifications from GR occur at values of  $M \simeq 2.0 M_\odot$ , close to the largest observed NS mass [35, 69]. Therefore from now on we will focus on EOS APR.

Notice that the first overtone is more sensitive to scalarization than the fundamental mode. This is confirmed in Fig. 6, where we show the frequencies of the  ${}_0 t_\ell$  and  ${}_1 t_\ell$  modes for a fixed stellar mass  $M = 1.8 M_\odot$  as a function of  $\beta$ . Newtonian estimates [67] (see also [7] for GR with similar conclusion), show that the overtones scale roughly as  $\approx n/\Delta\tilde{R}$  and are essentially independent of  $\ell$ , as long as  $\ell$  is not much larger than  $n$ . As shown by Eq. (25) and in Fig. 3, scalarization decreases the crust thickness. The shrinking crust thickness compensates for the reduced effective shear modulus, and the net effect is

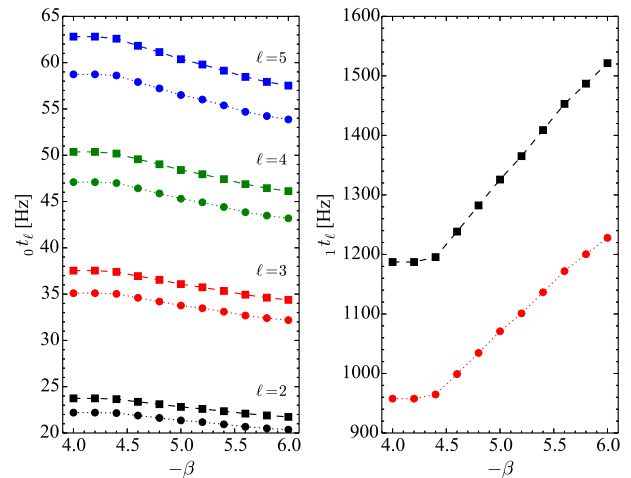


FIG. 6. (Color online) Frequencies of the torsional modes in scalar-tensor theory as a function of  $\beta$  for stellar models with mass  $M = 1.8 M_\odot$ . Circles and dotted lines correspond to APR+DH; squares and dashed lines correspond to APR+KP. In the right panel we plot the mode frequencies  ${}_0 t_\ell$  for  $\ell = 2, 3, 4$  and  $5$ . In the left panel we show the frequencies of the first overtone  ${}_1 t_\ell$ .

an increase of the oscillation frequencies. Notice also that in scalar-tensor theory the frequencies of the fundamental torsional oscillation mode decrease as we decrease  $\beta$  (the opposite happens in tensor-vector-scalar theory [49]).

In Fig. 7 we address the following question: are uncertainties in the EOS small enough to allow for tests of the underlying gravitational theory based on measurements of torsional oscillation frequencies in QPOs? Unfortunately, the answer is in the negative. Shaded regions in the plot are bounded by the values of the torsional oscillation frequencies computed using EOS DH and KP for the crust. One region (bounded by dashed lines) corresponds to GR, while the other (solid lines) to scalar-tensor theory. These regions are meant to roughly quantify the EOS uncertainty *within each theory*. Horizontal lines in the left panels mark the QPO frequency of 28 Hz observed in SGR 1900+14 [2], and identified with the  ${}_0 t_2$  mode. The plots show that for a theory parameter  $\beta = -4.5$  (marginally ruled out by binary pulsar observations [34]) the predictions of GR and scalar-tensor theory are indistinguishable within uncertainties in the crustal EOS. The bottom-left panel shows that, in principle, a scalar-tensor theory with  $\beta = -6.0$  could be distinguished from GR if we were to observe QPOs with frequencies smaller than 24 Hz in magnetars with  $M \gtrsim 1.6 M_\odot$ . However, such a large value of  $\beta$  is already excluded by binary pulsar experiments. The right panel carries out a similar analysis for the first overtone  ${}_1 t_\ell$ . The horizontal line indicates the QPO frequency of  $626.46 \pm 0.02$  Hz detected in SGR 1806-20 [3], and identified with the first overtone  ${}_1 t_\ell$ . The conclusions are similar: for  $\beta = -4.5$ , the predictions of GR and scalar-tensor theory are indistinguishable within uncertainties

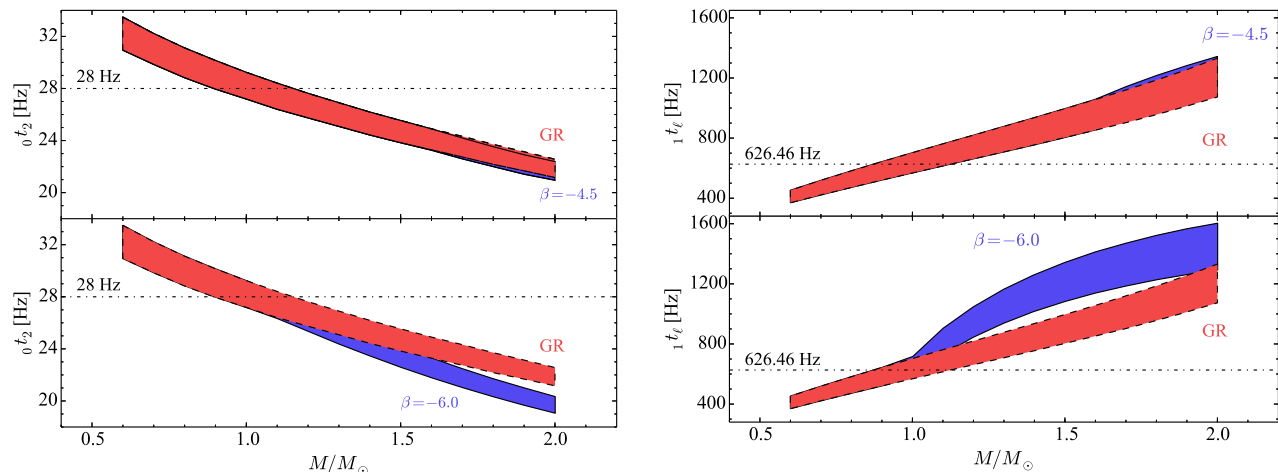


FIG. 7. (Color online) This plot compares modifications in torsional oscillation frequencies due to the underlying gravitational theory with crustal EOS uncertainties for models constructed using EOS APR in the core. Regions bounded by dashed lines correspond to oscillation frequencies in GR with different crustal EOSs; regions bounded by solid lines correspond to oscillation frequencies in scalar-tensor theory with different crustal EOSs. The degeneracy between modified gravity and crustal EOS is broken when the two regions do not overlap. Left panels refer to a scalar-tensor theory with  $\beta = -4.5$ , right panels to a theory with  $\beta = -6.0$  (a value already excluded by binary pulsar experiments [34]).

in the crustal EOS.

Let us now focus on the fundamental mode  ${}_0t_2$ , which has been identified with QPOs in both SGR 1900+14 ( $28 \pm 0.5$  Hz) [2] and SGR 1806-20 ( $30.4 \pm 0.3$  Hz) [3]. To quantify the relative effect of scalarization and electron screening, assuming the crustal EOS to be known, we introduce the ratio

$$\eta \equiv \frac{|{}_0t_2[\text{ST}] - {}_0t_2[\text{GR}]|}{|{}_0\bar{t}_2[\text{GR}] - {}_0t_2[\text{GR}]|}, \quad (51)$$

where  ${}_0t_2[\text{GR}]$  ( ${}_0t_2[\text{ST}]$ ) is the fundamental mode frequency in GR (scalar-tensor theory) ignoring electron screening, and  ${}_0\bar{t}_2[\text{GR}]$  is the corresponding frequency in GR computed by taking into account electron screening. Electron screening has a larger impact than scalarization whenever  $\eta < 1$ .

In Fig. 8 we show  $\eta$  as a function of the mass  $M$  for all combinations of core and crust EOS considered in this work. The punchline of this plot is consistent with our previous findings: the effect of electron screening is always dominant over scalarization for values of  $\beta$  that are compatible with current binary pulsar experiments. Unrealistically large values of  $\beta$  (e.g.,  $\beta = -6$ ) would be needed to constrain scalar-tensor theories via torsional oscillation frequencies.

## V. CONCLUSIONS

We studied torsional oscillations in NS crusts in scalar-tensor theories of gravity allowing for spontaneous scalarization. Working in the Cowling approximation, we showed that the “master equation” governing torsional

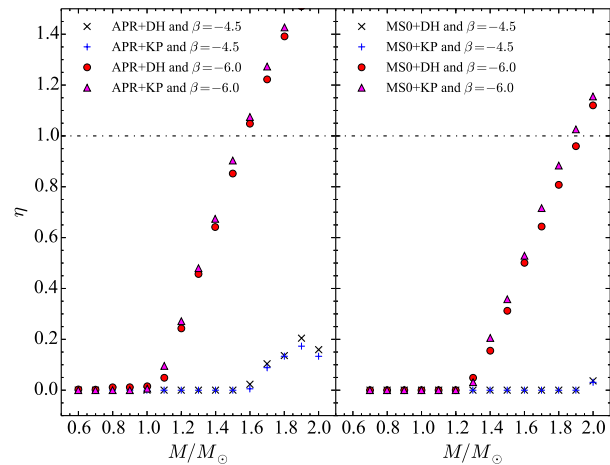


FIG. 8. (Color online) The ratio  $\eta$  defined in Eq. (51) for all stellar models considered in this work. Values of  $\eta > 1$  mean that the effect of scalarization is larger than that of electron screening. This would only be possible for values of  $\beta$  that are already ruled out by binary pulsar experiments.

oscillations – our Eq. (43) – has the same form as in GR [6] if we introduce an effective shear modulus  $\tilde{\mu}_{\text{eff}}$ , an effective wave velocity  $\tilde{v}_{\text{eff}}$  and a rescaled frequency  $\tilde{\omega}$ . In general, a smaller effective shear modulus reduces the oscillation frequencies. However we showed both analytically and numerically that the NS crust becomes thinner under scalarization, and a thinner crust tends to increase the overtone frequencies. Our numerical calculations show that the reduced shear modulus is the dominant effect for the fundamental mode, while the change

in crust thickness is dominant for the first overtone.

We found that the dominant torsional oscillation frequencies in scalar-tensor theory are essentially indistinguishable from those in GR for all values of  $\beta \geq -4.5$  that are still allowed by binary pulsar observations. One of the simplest microphysics effects that might affect the torsional oscillation frequencies, namely electron screening [15], has a much more important effect on torsional oscillation frequencies than scalarization. More noticeable deviations from GR would occur for (say)  $\beta = -6.0$ , but such large values of  $\beta$  are already ruled out by binary-pulsar observations [34]. We expect scalarization to be subdominant when compared to other uncertainties in the microphysics, such as nonuniform nuclear structures (pastas) [70] and superfluidity of dripped neutrons [11].

Given the similarities between torsional oscillation frequencies in GR and scalar-tensor theory, we can conjecture that the inclusion of slow rotation in our model will result in torsional modes growing due to the Chandrasekhar-Friedman-Schutz (CFS) instability [71]. The inclusion of slow rotation adds an extra term proportional to the frame dragging function  $\varpi$  (cf. [27]) in the perturbation equation (43). Previous studies of slowly rotating NSs in scalar-tensor theory [25] showed that scalarization affects  $\varpi$ , and therefore it will affect torsional modes for rotating stars.

One important omission in our study is the effect of magnetic fields, a crucial ingredient for realistic comparisons with QPO observations in magnetars. Very few works have studied NSs with magnetic fields in alternative theories of gravity (see e.g. [72]). Couplings between the scalar field and magnetic fields may produce larger deviations of the torsional oscillations frequencies with respect to GR. This is an interesting topic for future study.

## ACKNOWLEDGEMENTS

We are grateful to P. Pani for useful discussions and for validating some of our results. H. O. S., E. B. and M. H. were supported by NSF CAREER Grant No. PHY-1055103. H. S. was supported by Grant-in-Aid for Young Scientists (B) through JSPS Grant No. 26800133.

### Appendix A: Derivation of Eq. (25)

In this Appendix we present the derivation of Eq. (25). Making use of Eq. (13), we rewrite Eq. (15) as

$$\frac{d\tilde{p}}{dr} = -(\tilde{\varepsilon} + \tilde{p}) \left[ 4\pi A^4(\varphi) \frac{r^2 \tilde{p}}{r - 2m} + \frac{1}{2} r \psi^2 + \frac{m}{r(r - 2m)} + \alpha(\varphi) \psi \right]. \quad (\text{A1})$$

Let us assume that the following approximations hold true in the NS crust: (i)  $m_s \approx M$ , and therefore  $e^{-2\Lambda} = 1 - 2M/r_s$ ; (ii) the pressure  $\tilde{p}$  is negligible in comparison to  $\tilde{\varepsilon}$  [7]; (iii)  $\varphi \approx \varphi_s$  and  $\psi \approx \psi_s$ ; (iv)  $A(\varphi) \approx 1$ . We also

assume that the EOS has the polytropic form  $\tilde{\varepsilon} = k\tilde{p}^{1/\Gamma}$ , where  $k$  and  $\Gamma$  are constants. Then Eq. (A1) becomes

$$\frac{d\tilde{p}}{dr} \approx -\tilde{p} e^{2\Lambda} \frac{M}{r} - \tilde{\varepsilon} \left[ \frac{1}{2} r \psi_s^2 + \alpha(\varphi_s) \psi_s \right], \quad (\text{A2})$$

where  $\alpha(\varphi_s) = \beta\varphi_s$ . Integrating this equation from  $r = r_b$  to  $r = r_s$  and imposing  $\tilde{p}(r_s) = 0$  we obtain

$$0 = \sigma + M e^{2\Lambda} \left( \frac{1}{r_s} - \frac{1}{r_b} \right) - \psi_s^2 (r_s^2 - r_b^2) - \alpha(\varphi_s) \psi_s (r_s - r_b), \quad (\text{A3})$$

where we have defined  $\sigma \equiv \xi \tilde{p}_b / \tilde{\varepsilon}_b$  and  $\xi \equiv \Gamma / (\Gamma - 1)$  (recall that the subscript  $b$  denotes quantities evaluated at the crust basis).

We now make the additional assumption that  $\psi_s^2 (r_s^2 - r_b^2)$  is negligible compared to  $\alpha(\varphi_s) \psi_s (r_s - r_b)$ . We have verified this assumption by explicitly evaluating these two terms for different stellar models: typically  $\alpha(\varphi_s) \psi_s (r_s - r_b)$  is larger than  $\psi_s^2 (r_s^2 - r_b^2)$  by at least a factor 10.

Rewriting Eq. (A3) in terms of  $\mathcal{R}$  we obtain the quadratic equation

$$0 = \frac{\beta\xi}{\sigma} \mathcal{R}^2 - \left[ 1 + \frac{1}{\sigma} (\mathcal{C} e^{2\Lambda} + \beta\zeta) \right] \mathcal{R} + 1, \quad (\text{A4})$$

where we introduced  $\zeta = \zeta(\mathcal{C}) \equiv \varphi_s \psi_s r_s$ , which must be obtained by interpolation, given a family of stellar models, as a function of  $\mathcal{C}$ . Choosing the solution of Eq. (A4) that reduces to the GR result (24) when  $\beta \rightarrow 0$  and defining  $\mathcal{F} \equiv 1 + (\mathcal{C} e^{2\Lambda} + \beta\zeta) / \sigma$ , we finally obtain Eq. (25).

### Appendix B: Equivalence of the perturbation equations in Einstein and Jordan frames

Here we show that the perturbation equation (40) could also be obtained by starting with the energy-momentum conservation law in the Einstein frame,

$$\nabla_{*\mu} T_*^{\mu\nu} - \alpha(\varphi) T_* \nabla_*^\nu \varphi = 0.$$

For odd (axial) perturbations in the Cowling approximation, the perturbed Einstein-frame energy-momentum tensor  $\delta T_{*\mu\nu}$  satisfies

$$\partial_\mu \delta T_{*\nu}^\mu + \Gamma_{*\sigma\mu}^\mu \delta T_{*\nu}^\sigma - \Gamma_{*\nu\mu}^\sigma \delta T_{*\sigma}^\mu - \alpha(\varphi) \delta T_* \nabla_*^\nu \varphi = 0. \quad (\text{B1})$$

Using the relation  $T_{*\nu}^\mu = A^4(\varphi) \tilde{T}_\nu^\mu$  – which implies  $\delta T_{*\nu}^\mu = A^4(\varphi) \delta \tilde{T}_\nu^\mu$  – and the trace relation  $T_* = A^4(\varphi) \tilde{T}$ , we obtain upon substitution into Eq. (B1) that

$$4A^3(\varphi) \frac{A(\varphi)}{d\varphi} \partial_\mu \delta \tilde{T}_\nu^\mu + A^4(\varphi) \left[ \partial_\mu \delta \tilde{T}_\nu^\mu + \Gamma_{*\sigma\mu}^\mu \delta \tilde{T}_\nu^\sigma - \Gamma_{*\nu\mu}^\sigma \delta \tilde{T}_\sigma^\mu - \alpha(\varphi) \partial_\nu \varphi \delta \tilde{T} \right] = 0. \quad (\text{B2})$$

Dividing by  $A^4(\varphi)$  we recover Eq. (40).

- 
- [1] G. Israel, T. Belloni, L. Stella, Y. Rephaeli, D. Gruber, *et al.*, *Astrophys.J.* **628**, L53 (2005), arXiv:astro-ph/0505255 [astro-ph].
- [2] T. E. Strohmayer and A. L. Watts, *Astrophys.J.* **632**, L111 (2005), arXiv:astro-ph/0508206 [astro-ph].
- [3] T. E. Strohmayer and A. L. Watts, *Astrophys.J.* **653**, 593 (2006), arXiv:astro-ph/0608463 [astro-ph].
- [4] A. L. Watts, (2011), arXiv:1111.0514 [astro-ph.SR].
- [5] D. Huppenkothen, A. L. Watts, and Y. Levin, (2014), 10.1088/0004-637X/793/2/129, arXiv:1408.0734 [astro-ph.HE].
- [6] B. L. Schumaker and K. S. Thorne, *MNRAS* **203**, 457 (1983).
- [7] L. Samuelsson and N. Andersson, *Mon.Not.Roy.Astron.Soc.* **374**, 256 (2007), arXiv:astro-ph/0609265 [astro-ph].
- [8] H. Sotani, K. Kokkotas, and N. Stergioulas, *Mon.Not.Roy.Astron.Soc.* **375**, 261 (2007), arXiv:astro-ph/0608626 [astro-ph].
- [9] A. Colaiuda and K. D. Kokkotas, *Mon.Not.Roy.Astron.Soc.* **414**, 3014 (2011), arXiv:1012.3103 [gr-qc].
- [10] M. Gabler, P. C. Duran, N. Stergioulas, J. A. Font, and E. Muller, *Mon.Not.Roy.Astron.Soc.* **421**, 2054 (2012), arXiv:1109.6233 [astro-ph.HE].
- [11] H. Sotani, K. Nakazato, K. Iida, and K. Oyamatsu, *Mon.Not.Roy.Astron.Soc.* **428**, L21 (2013), arXiv:1210.0955 [astro-ph.HE].
- [12] A. T. Deibel, A. W. Steiner, and E. F. Brown, *Phys.Rev.* **C00**, 005800 (1969), arXiv:1303.3270 [astro-ph.HE].
- [13] K. Iida and K. Oyamatsu, *Eur.Phys.J.* **A50**, 42 (2014), arXiv:1309.1592 [nucl-th].
- [14] H. Sotani, K. Nakazato, K. Iida, and K. Oyamatsu, *Mon.Not.Roy.Astron.Soc.* **434**, 2060 (2013), arXiv:1303.4500 [astro-ph.HE].
- [15] H. Sotani, *Phys.Lett.* **B730**, 166 (2014), arXiv:1401.6977 [astro-ph.HE].
- [16] T. Damour and G. Esposito-Farese, *Phys.Rev.Lett.* **70**, 2220 (1993).
- [17] T. Harada, *Prog.Theor.Phys.* **98**, 359 (1997), arXiv:gr-qc/9706014 [gr-qc].
- [18] T. Harada, *Phys.Rev.* **D57**, 4802 (1998), arXiv:gr-qc/9801049 [gr-qc].
- [19] J. Novak, *Phys.Rev.* **D58**, 064019 (1998), arXiv:gr-qc/9806022 [gr-qc].
- [20] J. Novak and J. M. Ibanez, *Astrophys.J.* **533**, 392 (2000), arXiv:astro-ph/9911298 [astro-ph].
- [21] W. C. Lima, G. E. Matsas, and D. A. Vanzella, *Phys.Rev.Lett.* **105**, 151102 (2010), arXiv:1009.1771 [gr-qc].
- [22] P. Pani, V. Cardoso, E. Berti, J. Read, and M. Salgado, *Phys.Rev.* **D83**, 081501 (2011), arXiv:1012.1343 [gr-qc].
- [23] R. F. Mendes, G. E. Matsas, and D. A. Vanzella, *Phys.Rev.* **D89**, 047503 (2014), arXiv:1310.2185 [gr-qc].
- [24] T. Damour and G. Esposito-Farese, *Phys.Rev.* **D54**, 1474 (1996), arXiv:gr-qc/9602056 [gr-qc].
- [25] H. Sotani, *Phys.Rev.* **D86**, 124036 (2012), arXiv:1211.6986 [astro-ph.HE].
- [26] P. Pani and E. Berti, *Phys.Rev.* **D90**, 024025 (2014), arXiv:1405.4547 [gr-qc].
- [27] J. B. Hartle, *Astrophys.J.* **150**, 1005 (1967).
- [28] J. B. Hartle and K. S. Thorne, *Astrophys.J.* **153**, 807 (1968).
- [29] D. D. Doneva, S. S. Yazadjiev, N. Stergioulas, and K. D. Kokkotas, *Phys.Rev.* **D88**, 084060 (2013), arXiv:1309.0605 [gr-qc].
- [30] D. D. Doneva, S. S. Yazadjiev, N. Stergioulas, K. D. Kokkotas, and T. M. Athanasiadis, *Phys.Rev.* **D90**, 044004 (2014), arXiv:1405.6976 [astro-ph.HE].
- [31] D. D. Doneva, S. S. Yazadjiev, K. V. Staykov, and K. D. Kokkotas, (2014), arXiv:1408.1641 [gr-qc].
- [32] T. Damour and G. Esposito-Farese, *Class.Quant.Grav.* **9**, 2093 (1992).
- [33] T. Damour and G. Esposito-Farese, *Phys.Rev.* **D58**, 042001 (1998), arXiv:gr-qc/9803031 [gr-qc].
- [34] P. C. Freire, N. Wex, G. Esposito-Farese, J. P. Verbiest, M. Bailes, *et al.*, *Mon.Not.Roy.Astron.Soc.* **423**, 3328 (2012), arXiv:1205.1450 [astro-ph.GA].
- [35] J. Antoniadis, P. C. Freire, N. Wex, T. M. Tauris, R. S. Lynch, *et al.*, *Science* **340**, 6131 (2013), arXiv:1304.6875 [astro-ph.HE].
- [36] E. Barausse, C. Palenzuela, M. Ponce, and L. Lehner, *Phys.Rev.* **D87**, 081506 (2013), arXiv:1212.5053 [gr-qc].
- [37] M. Shibata, K. Taniguchi, H. Okawa, and A. Buonanno, (2013), arXiv:1310.0627 [gr-qc].
- [38] C. Palenzuela, E. Barausse, M. Ponce, and L. Lehner, *Phys.Rev.* **D89**, 044024 (2014), arXiv:1310.4481 [gr-qc].
- [39] L. Sampson, N. Yunes, N. Cornish, M. Ponce, E. Barausse, *et al.*, (2014), arXiv:1407.7038 [gr-qc].
- [40] K. Taniguchi, M. Shibata, and A. Buonanno, (2014), arXiv:1410.0738 [gr-qc].
- [41] K. Yagi and N. Yunes, *Science* **341**, 365 (2013), arXiv:1302.4499 [gr-qc].
- [42] K. Yagi and N. Yunes, *Phys.Rev.* **D88**, 023009 (2013), arXiv:1303.1528 [gr-qc].
- [43] H. Sotani and K. D. Kokkotas, *Phys.Rev.* **D70**, 084026 (2004), arXiv:gr-qc/0409066 [gr-qc].
- [44] H. Sotani and K. D. Kokkotas, *Phys.Rev.* **D71**, 124038 (2005), arXiv:gr-qc/0506060 [gr-qc].
- [45] H. Sotani, *Phys.Rev.* **D89**, 064031 (2014), arXiv:1402.5699 [astro-ph.HE].
- [46] H. Sotani, *Phys.Rev.* **D80**, 064035 (2009), arXiv:0909.2411 [gr-qc].
- [47] H. Sotani, *Phys.Rev.* **D79**, 064033 (2009), arXiv:0903.2424 [gr-qc].
- [48] H. Sotani, *Phys.Rev.* **D82**, 124061 (2010), arXiv:1012.2143 [astro-ph.HE].
- [49] H. Sotani, *Phys.Rev.* **D83**, 124030 (2011), arXiv:1106.3913 [astro-ph.HE].
- [50] H. Sotani, *Phys.Rev.* **D89**, 124037 (2014), arXiv:1406.3097 [astro-ph.HE].
- [51] N. Andersson, V. Ferrari, D. Jones, K. Kokkotas, B. Krishnan, *et al.*, *Gen.Rel.Grav.* **43**, 409 (2011), arXiv:0912.0384 [astro-ph.SR].
- [52] N. Andersson, J. Baker, K. Belczynski, S. Bernuzzi, E. Berti, *et al.*, *Class.Quant.Grav.* **30**, 193002 (2013), arXiv:1305.0816 [gr-qc].
- [53] A. Akmal, V. Pandharipande, and D. Ravenhall, *Phys.Rev.* **C58**, 1804 (1998), arXiv:nucl-th/9804027 [nucl-th].
- [54] H. Mueller and B. D. Serot, *Nucl.Phys.* **A606**, 508 (1996), arXiv:nucl-th/9603037 [nucl-th].

- [55] D. Kobayakov and C. Pethick, *Phys.Rev.* **C87**, 055803 (2013), arXiv:1303.1315 [nucl-th].
- [56] F. Douchin and P. Haensel, *Astron. Astrophys.* **380**, 151 (2001), arXiv:astro-ph/0111092 [astro-ph].
- [57] K. Kokkotas and J. Ruoff, *Astron.Astrophys.* **366**, 565 (2001), arXiv:gr-qc/0011093 [gr-qc].
- [58] E. Berti, F. White, A. Maniopolou, and M. Bruni, *Mon.Not.Roy.Astron.Soc.* **358**, 923 (2005), arXiv:gr-qc/0405146 [gr-qc].
- [59] L. Samuelsson, *Stellar Models in General Relativity* (Ph.D. Thesis, Stockholm University).
- [60] P. N. McDermott, H. M. van Horn, and J. F. Scholl, *ApJ* **268**, 837 (1983).
- [61] L. S. Finn, *MNRAS* **232**, 259 (1988).
- [62] S. L. Shapiro and S. A. Teukolsky, *Black Holes, White Dwarfs, and Neutron Stars: the Physics of Compact Objects* (John Wiley, 1983).
- [63] N. Chamel and P. Haensel, *Living Rev.Rel.* **11**, 10 (2008), arXiv:0812.3955 [astro-ph].
- [64] S. Ogata and S. Ichimaru, *Phys. Rev. A* **42**, 4867 (1990).
- [65] T. Strohmayer, H. M. van Horn, S. Ogata, H. Iyetomi, and S. Ichimaru, *ApJ* **375**, 679 (1991).
- [66] C. Horowitz and J. Hughto, (2008), arXiv:0812.2650 [astro-ph].
- [67] C. J. Hansen and D. F. Cioffi, *ApJ* **238**, 740 (1980).
- [68] N. Messios, D. B. Papadopoulos, and N. Stergioulas, *Mon.Not.Roy.Astron.Soc.* **328**, 1161 (2001), arXiv:astro-ph/0105175 [astro-ph].
- [69] P. Demorest, T. Pennucci, S. Ransom, M. Roberts, and J. Hessels, *Nature* **467**, 1081 (2010), arXiv:1010.5788 [astro-ph.HE].
- [70] H. Sotani, *MNRAS* **417**, L70 (2011), arXiv:1106.2621 [astro-ph.HE].
- [71] M. Vavoulidis, A. Stavridis, K. Kokkotas, and H. R. Beyer, *Mon.Not.Roy.Astron.Soc.* **377**, 1553 (2007), arXiv:gr-qc/0703039 [GR-QC].
- [72] A. Hakimov, A. Abdujabbarov, and B. Ahmedov, *Phys.Rev.* **D88**, 024008 (2013).